Original

Srinivasan, A.; Huang, Y.; Mendis, C.; Dieringa, H.; Blawert, C.; Kainer, K.U.; Hort, N.:

Microstructure, Mechanical and Corrosion Properties of Mg-Gd-Zn Alloys

Materials Science Forum, Light Metals Technology Conference, LMT 2013 (2013)
Trans Tech Publications

DOI: 10.4028/www.scientific.net/MSF.765.28

Materials Science Forum Vol. 765 (2013) pp 28-32

doi:10.4028/www.scientific.net/MSF.765.28

Microstructure, Mechanical and Corrosion Properties of Mg-Gd-Zn Alloys

A. Srinivasan[1,2,a], Y. Huang[1,b], C. L. Mendis[1,c], H. Dieringa[1,d], C. Blawert[1,e], K. U. Kainer[1,f] and N. Hort[1,g]

[1]Helmholtz-Zentrum, Geesthacht, Institute of Materials Research, Max-Planck-Str. 1, 21502 Geesthacht, Germany

[2]National Institute for Interdisciplinary Science and Technology, CSIR, Pappanamcode (P.O) Thiruvananthapuram 695 019, India

[a]srininiist@gmail.com, [b]yuanding.huang@hzg.de, [c]chamini.mendis@hzg.de, [d]hajo.dieringa@hzg.de, [e]carsten.blawert@hzg.de, [f]karl.kainer@hzg.de, [g]norbert.hort@hzg.de

Keywords: Mg-Gd-Zn alloys, $(Mg,Zn)_3Gd$, LPSO, Tensile properties, Creep, Corrosion behaviour

Abstract. Microstructure, mechanical and corrosion properties of Mg-10Gd-2Zn and Mg-10Gd-6Zn (all in wt.%) were evaluated in the as-cast condition. The microstructures of both alloys contained $(Mg, Zn)_3Gd$ phase at the interdendritic regions and long period stacking ordered (LPSO) phase distributed in the matrix. The Mg-10Gd-6Zn alloy consisted of a high volume fraction of $(Mg,Zn)_3Gd$ intermetallic phases continuously distributed along the grain boundaries. The tensile properties, especially the elongation to failure of the Mg-10Gd-6Zn alloy were slightly lower than those of Mg-10Gd-2Zn. An enhancement in creep resistance was observed with Mg-10Gd-2Zn alloy with the post creep tested microstructure showing dynamic precipitation. Corrosion studies indicated that increased Zn content, from 2 to 6 % in Mg-10Gd alloys, significantly reduced the corrosion resistance.

Introduction

Recently, development of magnesium alloys with heavy as well as highly soluble rare earth (RE) metals such as Gd, Dy etc. have become an interesting subject for scientific investigations. Gd is one such rare earth element, that is being investigated for the possible development of new magnesium alloys with enhanced mechanical and corrosion properties. It has been reported that binary Mg-Gd alloys have better creep resistance than that of the commercial WE43 and QE22 alloys [1]. Many experimental alloys based on Mg-Gd-Y, Mg-Gd-Y-Nd, Mg-Gd-Zn, Mg-Gd-Y-Zn etc. have been developed and their microstructure and properties investigated. Among these systems, Mg-Gd-Zn is one of the very important systems as its microstructure consists of many different phases, such as I, W, Z and laves phases, depending upon the ratio of Zn and Gd contents, thus resulting in different mechanical behaviours [2]. In the present study, microstructure, mechanical and corrosion properties of Mg-10Gd-2Zn and Mg-10Gd-6Zn were evaluated in the as-cast condition, and the properties were correlated with their microstructures.

Experimental

The alloys, Mg-10Gd-2Zn (Alloy 1) and Mg-10Gd-6Zn (Alloy 2) (all in wt.%), for the present investigation were prepared in a resistance tilt furnace under a protective gas mixture of Ar + 2% SF_6. Polished samples were examined with optical, scanning electron (SEM) and transmission electron (TEM) microscopes. Tensile samples with a 30 mm gauge length, 6 mm diameter and M10 threads were machine out from the castings, and tested at room (RT) and at elevated temperatures of 200 and 230 ^oC according to DIN EN 10002 with a strain rate of 1×10^{-3} s^{-1}. Creep tests were conducted at 250 and 300 ^oC with different initial stresses. Corrosion tests were conducted at room temperature in 0.5 wt.% NaCl solution using standard eudiometer apparatus with a total volume of 400 ml and a resolution of 0.5 ml. Cubic samples of size 14 x14 x 14 mm^3 were used for eudiometer

studies. The corrosion rate (CR) was calculated in mm per year by converting the total amount of collected hydrogen into material loss (1 ml H_2 gas = 0.001083 g dissolved Mg) using the following equation:

$$CR = \frac{8.76 \times 10^4 \times \Delta g}{A \cdot t \cdot \rho} \quad (1)$$

where Δg is total weight loss in g, A is surface area of the sample exposed in cm^2, t is total immersion time in h and ρ is the density of the alloy in g cm^{-3}

Results and Discussion

Microstructures. Fig. 1a&b, show the SEM and TEM micrographs of Alloy 1, respectively. Two types of second phases were seen at the interdendritic regions, and the EDS analysis of the major phase marked as 'A' in Fig. 1a indicated that the phase consistently contained a little higher Gd than Zn content. The typical composition of the phase was 56.97 at.% Mg, 21.97 at.% Gd, 19.47 at.% Zn. The TEM analysis confirmed that the phase was face centred cubic (fcc) Mg_3Gd type compound with the lattices parameter a = 0.726 nm. Thus, it can be identified as $(Mg,Zn)_3Gd$ type phase as reported in the literature [3]. This phase was previously referred to as W phase in the literature [4]. A few small particles (marked as 'B' in Fig. 1a) containing equal amounts of Gd and Zn content (81.49 at.% Mg, 8.62 at.% Gd, 8.72 at.% Zn), but with lower volume fraction as compared to the $(Mg,Zn)_3Gd$ phase, were also seen. This phase is similar to the $Mg_{12}GdZn$ type phase, which is normally referred as Z or X phase containing LPSO structure. In addition, lamellar LPSO phase in the α-Mg matrix was also observed as evident from Fig. 1b. The microstructure of Alloy 2 consisted of a continuous network of second phase particles (Fig. 1c). The EDS spectra taken at different particles showed that the Zn content was little higher than the Gd content and the Zn/Gd ratio was close to 1.5. From the TEM analysis it was confirmed that the phase was Mg_3Gd type with a lattice parameter, a = 0.732 nm. Hence, this phase can be identified as $(Mg,Zn)_3Gd$ phase similar to the phase observed in Alloy 1, but with slightly different lattice parameters and formed as a more continuous network at the interdendritic regions. The TEM investigation also confirmed the presence of fine lamellar LPSO phase in the matrix. Moreover, no significant difference in the size of the lamellar LPSO phases in the two alloys was noticed.

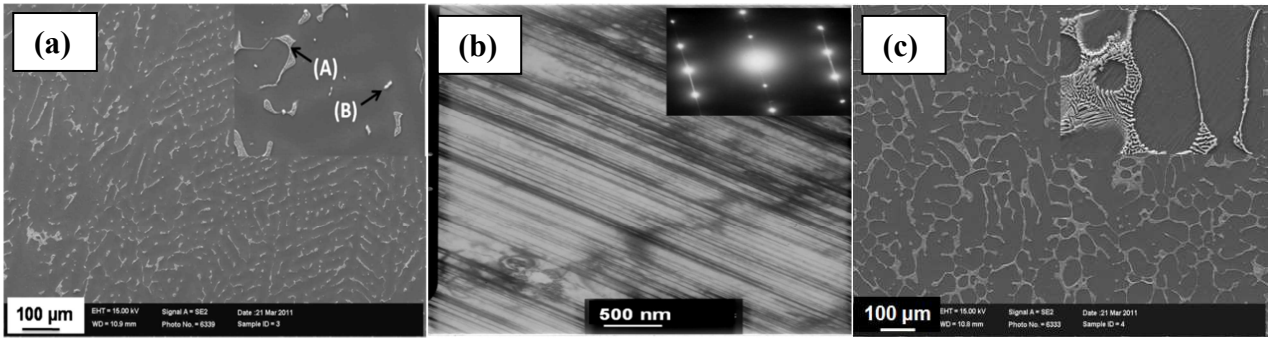

Fig. 1. Microstructures of (a, b) Alloy 1, (c) Alloy 2.

Tensile Properties. The tensile properties of the alloys at room temperature as well as at high temperatures are given in Table 1. In general, the yield and the tensile strengths of both alloys were similar; however, the elongation to failure of Alloy 2 was lower. The elongation to failure of Alloy 2 was 34 % lower than that of Alloy 1 at room temperature. From the microstructures of Alloy 1 and Alloy 2 it can be seen that with the increase in Zn content from 2 to 6 % the amount of secondary phase at the grain boundaries increased and became continuous. The second phase (W phase/$(Mg,Zn)_3Gd$)) in Mg-Gd-Zn alloys is incoherent with the Mg matrix, which leads to the formation of a weak interface [5]. For good particle strengthening at the grain boundary, the

interface between the particle and the matrix should be coherent. Pile up of dislocations at the interface leads to the initiation of cracks and easier propagation along the interfaces, which results in poor ductility. In the present study, the TEM investigation suggested that the $(Mg,Zn)_3Gd$ phase had an f.c.c. structure leading to poor lattice matching, and the increased volume fraction of continuous second phase at the boundaries in Alloy 2 led to the inferior tensile properties. As the test temperature increased to 200 °C, the TYS and ultimate tensile strength (UTS) decreased significantly whereas elongation increased slightly for both alloys. Further increase in test temperature, i.e. to 230 °C, did not alter the tensile properties significantly. At all test temperatures, the yield strength and tensile strength was higher in Alloy 1 compared with Alloy 2.

Table 1. Tensile properties of alloys at RT and high temperatures (the S.D values are given in parenthesis).

Alloys	Testing temp. [°C]	TYS [MPa]	UTS [MPa]	%Elongation
Alloy 1	RT	118.03 (1.77)	144.90 (4.30)	1.36 (0.28)
	200	94.83 (3.06)	127.23 (3.10)	2.03 (0.33)
	250	92.17 (2.12)	131.08 (1.97)	3.02 (0.52)
Alloy 2	RT	116.73 (3.47)	143.62 (6.06)	0.90 (0.26)
	200	90.55 (2.18)	127.47 (6.12)	2.03 (0.71)
	250	84.56 (2.62)	125.93 (6.67)	2.60 (0.65)

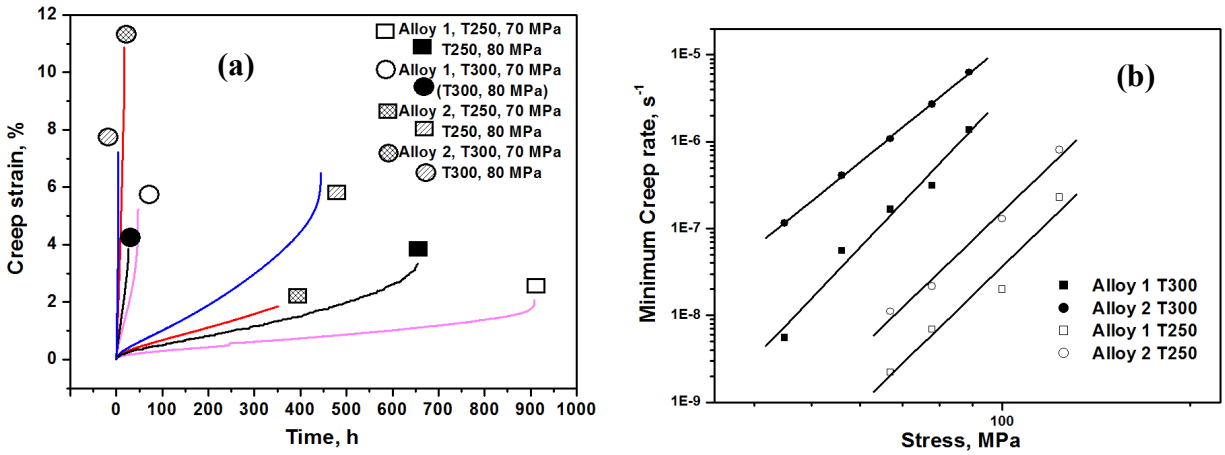

Fig. 2. (a) Creep curves of the alloys, (b) logarithmic stress versus minimum creep rate plots.

Creep Behaviour. Fig. 2a shows typical creep curves of the alloys tested at 250 and 300 °C under 70 and 80 MPa initial stress. It was seen that the creep performance of Alloy 1 was better than that of Alloy 2 at all the tested temperature and stress conditions. The minimum creep rates of Alloy 2 (Table 2) were one order of magnitude higher than those of Alloy 1. These results clearly indicate that the increase in Zn content in Mg-10Gd alloy from 2 to 6 %, significantly changed the creep behaviour of the alloy. The logarithmic stress versus minimum creep rate plots for the alloys at 250 and 300 °C are shown in Fig. 2b. It can be seen that the calculated n value changed from 8.4 (at 250 °C) to 8.8 (at 300 °C) for Alloy 1, whereas it changed from 7.4 (at 250 °C) to 6.8 (at 300 °C) for Alloy 2. Similarly, the calculated Q values were 215-190 KJ/mol for Alloy 1 and 228-240 KJ/mol for Alloy 2. The post creep test microstructural analyses indicated the presence of coarse β precipitates in Alloy 1 after creep testing at 250 °C as shown in Fig. 3a. However, no such precipitates were seen in Alloy 2 (not shown here). This indicated that Alloy 1 was strengthened by dynamic precipitation during creep exposure at low temperature. Also, such precipitation did not occur at the high temperature (300 °C). The EDS analysis of the as cast samples showed that Alloy 1 contains Gd rich areas around the second phase, and the β precipitates form during creep. However, no such regions were seen in Alloy 2, which was due to the presence of higher Zn content

(6%) that led to increased amount of second phase (Fig. 1c) and lower supersaturation of solute in the inter-dendritic regions during solidification. At higher temperature (300 ^{o}C), the deformation was concentrated in the LPSO phase in both alloys as shown in Fig. 3b.

Table 2. Minimum creep rates of the alloys under different creep conditions.

	Minimum creep rate, [s^{-1}] at 250 ^{o}C				Minimum creep rate, [s^{-1}] at 300 ^{o}C			
Stress [MPa]	70	80	100	120	50	60	70	80
Alloy1	$2.2X10^{-9}$	$6.9X10^{-9}$	$2X10^{-8}$	$2.3X10^{-7}$	$5.6X10^{-9}$	$5.6X10^{-8}$	$1.7X10^{-7}$	$3.1X10^{-7}$
Alloy 2	$1.1X10^{-8}$	$2.2X10^{-8}$	$1.3X10^{-7}$	$8X10^{-7}$	$1.2X10^{-7}$	$4X10^{-7}$	$1.1X10^{-6}$	$2.7X10^{-6}$

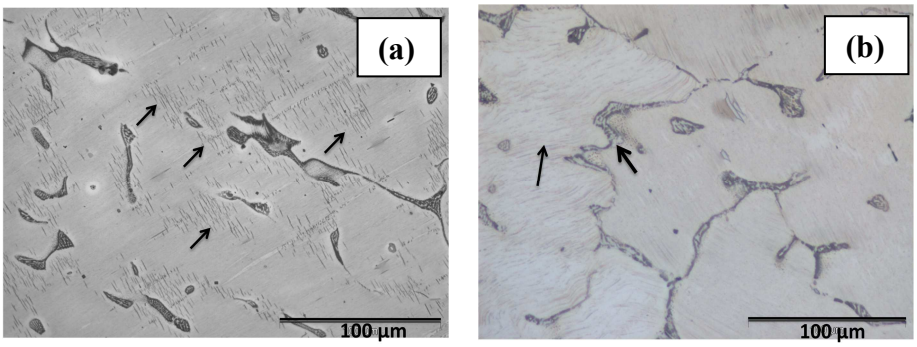

Fig. 3. Microstructures of Alloy 1 subjected to creep (a) at 250 ^{o}C, 80 MPa, (b) at 300 ^{o}C, 70 MPa.

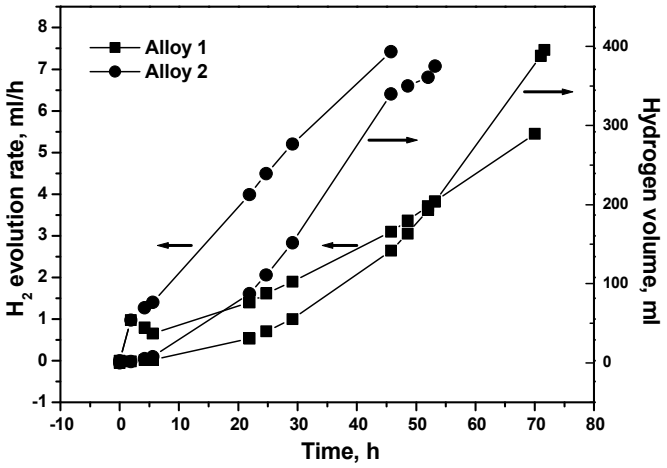

Fig. 4. Hydrogen volumes and its evolution rates of the alloys during corrosion.

Corrosion Properties. The hydrogen evolution curves for the different alloys are shown in Fig. 4. The volume of hydrogen increased with increasing time for both of the alloys, but at different rates. The rate of increase in hydrogen volume in Alloy 1 was slow compared to that in Alloy 2. The corrosion rates of Alloy 1 and Alloy 2 calculated from the hydrogen volumes were 23.50 mm/yr and 32.29 mm/yr, respectively. This result clearly indicates that the corrosion rate increased as the Zn content in the alloy increased. In general most of the second phases in the magnesium alloys are nobler than the magnesium matrix. These noble second phases at the grain boundary form a galvanic couple with the matrix and act as cathodic sites during corrosion. RE additions, as a major alloying element in Mg such as Mg-La, Mg-Ce, Mg-Nd and Mg-Y, lead to increased corrosion rates due to the presence of second phases [6]. Previous studies also reported that these galvanic effects due to the second phases reduce the corrosion resistance of Mg-RE-Y and Mg-RE-Zn ternary alloys, and when the second phases are dissolved into the matrix by solution treatment the corrosion

properties improve drastically as the presence of rare earth elements in the solid solution stabilizes the surface film [7]. Hence the higher corrosion rate observed in Alloy 2 can be attributed to the higher volume fraction of second phases. Detailed investigation is in progress to confirm this mechanism.

Conclusions

The microstructures of Mg-10Gd-2Zn and Mg-10Gd-6Zn contained $(Mg,Zn)_3Gd$ and LPSO phases; however, the volume fraction of second phase was higher in Mg-10Gd-6Zn. Mg-10Gd-2Zn alloy showed better tensile and corrosion properties. Dynamic precipitation occurred in the Mg-10Gd-2Zn alloy which improved its creep properties.

Acknowledgements

The authors thank Mr. G. Meister for the preparation of alloys, Mrs. Petra Fischer for SEM, Dr. Jan Bohlen for tensile test. The first author also acknowledges the Alexander von Humboldt (AvH) foundation for the fellowship and the Director, CSIR-NIIST for granting deputation to HZG to carry out the work.

References

[1] B.L. Mordike, Creep-resistant magnesium alloys, Mat. Sci. Eng. A 324 (2002) 103-112.

[2] S. Zhang, G.Y. Yuan, C. Lu, W.J. Ding, Effect of Zn/Gd ratio on phase constitutions in Mg-Zn-Gd alloys, in: Wim H. Sillekens, Sean R. Agnew, Neale R. Neelameggham and Suveen N. Mathaudhu (Eds.), Magnesium Technology 2011, John Wiley & Sons, Inc., New Jersey, 2011, pp. 157-159.

[3] M. Yamasaki, M. Sasaki, M. Nishijima, K. Hiraga, Y. Kawamura, Formation of 14H long period stacking ordered structure and profuse stacking faults in Mg-Zn-Gd alloys during isothermal aging at high temperature, Acta Mater. 55 (2007) 6798-6805.

[4] Y. Liu, G. Yuan, C. Lu, W. Ding, Stable icosahedral phase in Mg-Zn-Gd alloy, Scripta Mater. 55 (2006) 919-922.

[5] D.K. Xu, L. Liu, Y.B. Xu, E.H. Han, Effect of microstructure and texture on the mechanical properties of the as-extruded Mg-Zn-Y-Zr alloys, Mat. Sci. Eng. A 443 (2007) 248-256.

[6] N. Birbilis, M.A. Easton, A.D. Sudholz, S.M. Zhu, M.A. Gibson, On the corrosion of binary magnesium-rare earth alloys, Corros. Sci. 51 (2009) 683-689.

[7] R. Pinto, M.G.S. Ferreira, M.J. Carmezim, M.F. Montemor, Passive behaviour of magnesium alloys (Mg-Zr) containing rare-earth elements in alkaline media, Electrochim. Acta 55 (2010) 2482-2489.